Int. J. Electrochem. Sci., 14 **(2019)** 7104 – 7115, doi: 10.20964/2019.08.29

International Journal of
ELECTROCHEMICAL
SCIENCE
www.electrochemsci.org

Preparation of Pt-Pd/PANI/Graphene Nanosheets Composites as Electrocatalysts for Direct Methanol Fuel Cell

Ling Shi[1,2], *Zefeng Wang*[1,2,*], *Xianlan Chen*[1,2], *Guangming Yang*[1,2,*], *Wei Liu*[1,2,]

[1] School of science, Honghe University, mengzi,Yunnan 661199, PR China
[2] Key Laboratory of Natural Pharmaceutical & Chemical Biology of Yunnan Province, Mengzi, Yunnan 661199, PR China
[*]E-mail: wangzefeng841006@163.com; yangguangmingbs@126.com

Received: 4 April 2019 / *Accepted:* 17 May 2019 / *Published:* 30 June 2019

The synthesis of noble metal nanoparticle with controlled shapes is an attractive goal in developing highly active catalysts. However, constructing high-quality noble metallic nanocatalysts with good electrocatalytic activity remains a huge challenge to date. In this research work, the high-quality polyaniline functionalized graphene nanosheets (PANI/GNS) were prepared by an interfacial polymerization method. The abundant -NH_2 groups onto the surface of resulted PANI/GNS nanocomposites, and can be used as active site for growing high load rate of Pd nanoparticles (NPs). Subsequently, Pt NPs were successfully deposited on the Pd surface formed Pt-Pd/PANI/graphene nanosheets (Pt-Pd/PANI/GNS) composites. Interestingly, the shape of Pt-Pd bimetallic can be effectively controlled *by* simply changing the reaction parameters. The shape and structure of nanocatalysts were characterized by X-ray diffraction (XRD) and transmission electron microscopy (TEM). The electrocatalytic properties of nanocomposites were characterized by cyclic voltammetry (CV). The TEM images show that the Pt-Pd nanoflowers were successfully decorated onto the surface of PANI/GNS nanocomposites. The electrocatalytic properties for dioxygen and methanol of prepared Pt-Pd/PANI/GNS nanocatalyst were investigated. The electrochemical results show that the nanocatalysts exhibit higher electrocatalytic activity for methanol oxidation and dioxygen reduction.

Keywords: Graphene; Polyaniline; Pd-Pt Bimetallic; Direct Methanol Fuel Cell

1. INTRODUCTION

The electrochemical properties of monometallic nanoparticles are prone to being influenced by the shapes and sizes of nanoparticles in fuel cell field. Significant efforts have been focus on effectively designing the nannostructures of Pt nanocatalysts so as to improve their activity and enhancing catalytic properties. Crucial efforts have been directed towards preparing Pt-based multifunctional hybrid nanostructures. Prominent examples include flowerlike structures Pt-Au bimetallic electrochemically

deposited on the surface of the graphene/GC [1], Pt was grown on the surface of ultrathin SnS_2 nanoplate *via* in situ reduction of a Pt salt [2], Pt/CeO_2/PANI nanorod arrays were designed as advanced electrocatalysts for methanol oxidation [3], the Pt-on-Pd bimetallic nanodendrites supported on graphene nanosheets were prepared by wet-chemical approach [4]. The obtained dendritic nanoparticles exhibited excellent electrocatalytic activity. Therefore, designing Pt-based nanodendrite as catalyst is a significant challenge in fuel cell field. In order to increase the electrochemical activity of Pt NPs and reduce the dosage of Pt NPs, Pt-based alloy nanoparticles have received great interest in recent years [5].

Graphene nanosheet (GNS) has obtained much interest due to its high conductivity and large surface area. GNS can be prepared relatively easily by chemical reduction graphite oxide. GNS has obtained considerable attention in electrochemical sensors due to its abundant interactive functions at the surface [6]. Unfortunately, the GNS has high hydrophobic property, generally form irreversible agglomerates or even restack to form graphite through strong π-π stacking interaction [7]. The poor water-soluble of graphene will limit the application of graphene. Hence, the method of dispersing GNS was developed by introducing the hydrophilic groups on graphene surface [8,[9]. Recently, many researches had focused on improving its solubility/processability by functionalization of graphene. For example, Cheng's group [10] prepared the ionic liquid functionalized graphene nanoplatelet and reduced graphene oxide. Zahl's group [11] reported that the phenyl-modified graphene nanoribbons and prove that the graphene nanoribbons can be used as atomically precise graphene nanopores. Ruoff's group [12] prepared stable aqueous dispersions of polymer-functionalized graphitic nanoplatelets via the reduction of exfoliated graphite oxide. Therefore, design a water-soluble molecule to functionalize GN in order to take advantages of both functionalizing material and superior properties of graphene is a significant challenge.

Conductive polymer with conjugated system structure can be used as functional molecular that can functionalize graphene through conjugate action. Among those conductive polymers, polyaniline (PANI) as a conducting polymer has been immensely researched in sensors [13], antibacterial [14], batteries [15] due to its attractive properties, such as excellent conductivity, easy synthesis, excellent redox sensitivity, and tunable chemical properties. A variety of studies have been engaged to synthesize PANI through template-assisted polymerization, chemical oxidation polymerization, interfacial polymerization, seeding polymerization, etc [14]. In order to obtain excellent properties of PANI functionalize graphene. The conductivity and shape of functional molecular PANI is the key factor responsible for the prepared composites. Liquid-liquid interfacial polymerization method as a new and simple fool-proof approach can be obtained high quality PANI.

In this paper, we demonstrate a novel liduid-liquid interface polymerization method for synthesizing of polyaniline/graphene nanosheets (PANI/GNS). The PANI can effectively improve the dispersity of GNS. Next, Pt-Pd bimetallic nanoflowers decorated on polyaniline/graphene nanosheets (Pt-Pd/PANI/GNS) were obtained by a wet-chemical approach. The structure and morphology of Pt-Pd/PANI/GNS nanocatalysts were characterized by transmission electron microscopy (TEM), powder X-ray diffraction (XRD). Interestingly, the shapes and the catalytic performance of Pt-on-Pd bimetallic were easily tuned by changing the additive amount of H_2PtCl_6. The as-prepared Pt-Pd/PANI/GNS nanocatalyst possessed good synergistic effects of the Pt-Pd bimetallic nanoflowers and PANI/GNS composites, making the 3D Pt-Pd/PANI/GNS nanocatalyst exhibit attractive electrocatalytic activity.

2. EXPERIMENTAL

2.1 Materials

Graphite flake (99.8%, 8000 mesh) was provided by aladdin. Hexachloroplatinic (IV) acid hexahydrate ($H_2PtCl_6 \cdot 6H_2O$) and K_2PdCl_4 were purchased from the Shanghai sybridge Chemical Reagent Company. Poly(N-vinyl-2-pyrrolidone) (PVP K30, molecular weight=30000~40000), CH_2Cl_2, HCl, HCOOH, $FeCl_3 \cdot 6H_2O$, H_2O_2, CH_2Cl_2 were purchased from Sinopharm group reagent co. LTD. The aniline was fresh distillation prior to use. All aqueous solutions were prepared with doubly distilled water.

2.2 Apparatus

Transmission electron microscopy (TEM) and high resolution TEM (HRTEM) measurements were made on a JEM-2100 transmission electron microscope (JEOL Ltd.). The X-ray diffraction (XRD) graphs of the prepared nanomaterials are analyzed on X'Pert^3 powder diffractometer (PANAlytical Company) operating at 40 mA and 40 kV using Cu-Kα as radiation source.

2.3 Preparation of PANI/GNS nanocomposites

Graphite oxide (GO) was prepared from graphite using a modified Hummers method [16,[17]. PANI/GNS composites were prepared by an interfacial polymerization method according to our previous works [18]. The interfacial polymerization reaction was carried out in a 200 mL reaction flask in which 50 mL of aniline was dispersed in 50 mL CH_2Cl_2 to form the lower organic phase. 1.5 mg of GNS and 50 mg of $FeCl_3 \cdot 6H_2O$ were dissolved in 50 mL of 1 M HCl by sonicating for 2 h, and mildly added to the organic phase containing aniline and CH_2Cl_2. After the interfacial system was established, the polymerization reaction was kept at 37°C for about 48 h, until the polymerization reaction is completed. The obtained sample was centrifuged and washed several times with double-distilled water until it became neutral. The obtained PANI/GNS composites were redissolved in double-distilled water.

2.4 Preparation of Pd/PANI/GNS hybrids

0.5 mg of PANI/GNS composites were dispersed in 1.5 mL double-distilled water, followed by the addition of 0.7 mL of 20 mM K_2PdCl_4 by sonicating for 20 min, followed by addition of 0.35 mL HCOOH. The mixtures were stirred at room temperature for more than 24 h until the K_2PdCl_4 was reduced completely. Then, the obtained solution was centrifuged and washed several times with double-distilled water and dissolved in 3.8 mL of water.

2.5 Preparation of Pt-Pd Bimetallic Nanoflowers Supported on Polyaniline/Graphene Hybrids

The Pt-Pd bimetallic nanoflowers decorated on PANI/GNS nanocatalysts were prepared by the protocol reported in the literature [4]: 3.8 mL of Pd/PANI/GNS hybrids, 0.25 mL of 1 M PVP aqueous solution, and 0.26 mL of 0.193 M $H_2PtCl_6 \cdot 6H_2O$ were added into a 10 mL flask. The solution was stirred vigorously for 20 min. 0.5 mL HCOOH was added into the above solution in air under magnetic stirring. The reaction was carried out at room temperature until the Pt precursor was reduced completely. The obtained products were collected by centrifugation and washed several times with double-distilled water. The obtained product was denoted as sample 1.

2.6 Electrocatalytic Experiment

The electrocatalytic experiments of nanocatalysts were measured on electrochemical analyzer, CHI660E. A glassy carbon electrode (GCE, 3 mm) was used as the working electrode, Pt wire was used as the counter electrode and saturated calomel electrode (SCE) was used as the reference electrode. The obtained nanocatalysts were dispersed in double-distilled water by vigorous sonication. The concentration of nanocatalyst was adjusted to 1 mg/mL, then 7 μL of nanocatalysts were deposited on the GCE. Subsequently, Nafion solution (3 μL, 0.3%) was coated onto the electrocatalysts on the GCE surface. Electrochemically active surface area (ECSA) of Pt-Pd/PANI/GNS nanocatalyst was measured by cyclic voltammetry (CV) in a N_2-saturated 0.5 M H_2SO_4 solution at scan rate of 50 mV/s. ECSA was calculated from hydrogen desorption peak area between -0.2 and +0.4 V. The electrooxidation and stability of methanol was performed by cyclic voltammograms in a mixing solution containing 1 M CH_3OH and 0.5 M H_2SO_4. The oxygen reduction reaction was performed by CV in O_2-saturated aqueous 1.0 M H_2SO_4.

3. RESULT AND DISCUSSION

3.1 Characterization of nanocatalysts

Transmission electron micrographs of prepared nanomaterials are shown in Figure 1. Figure 1A shows the TEM image of GNS, revealing the flakelike and thin of grapheme nanosheets. Additionally, the crumpled silk waves are observed when PANI is polymerized onto the surfaces of the GNS in Figure 1B. The shape of PANI/GNS nanocomposite film is similar to the PANI. That maybe due to the type of oxidant in the process of preparation of PANI functionalized GNS, $FeCl_3$ is a milder oxidant when aniline oxidative polymerization. Firstly, aniline monomer is adsorbed on graphene surface by electrostatic adsorption. Then aniline was oxidized polymerization into uniform PANI films and grown onto the surface of GNS under the presence of mild oxidizer. In this method, the liquid-liquid interface polymerization method provides an excellent template for the polymerization of aniline onto the surface of GNS. Figure 1C shows the images of Pd/PANI/GNS nanohybrids. A large of ultrafine and uniformly disperse Pd nanoparticles were deposited onto the surface of PANI/GNS substrate. The graphene nanosheets have large surface area, and the both sides can be decorated by Pd nanoparticles. The HRTEM image of the Pd/PANI/GNS nanohybrid (Figure 1D) shows that the Pd nanoparticles have an

average size of 2.5 nm. Moreover, the HRTEM images show that the detailed crystalline structure of the GNS. The graphitic layers are curved, interrupted and have many defects [19].

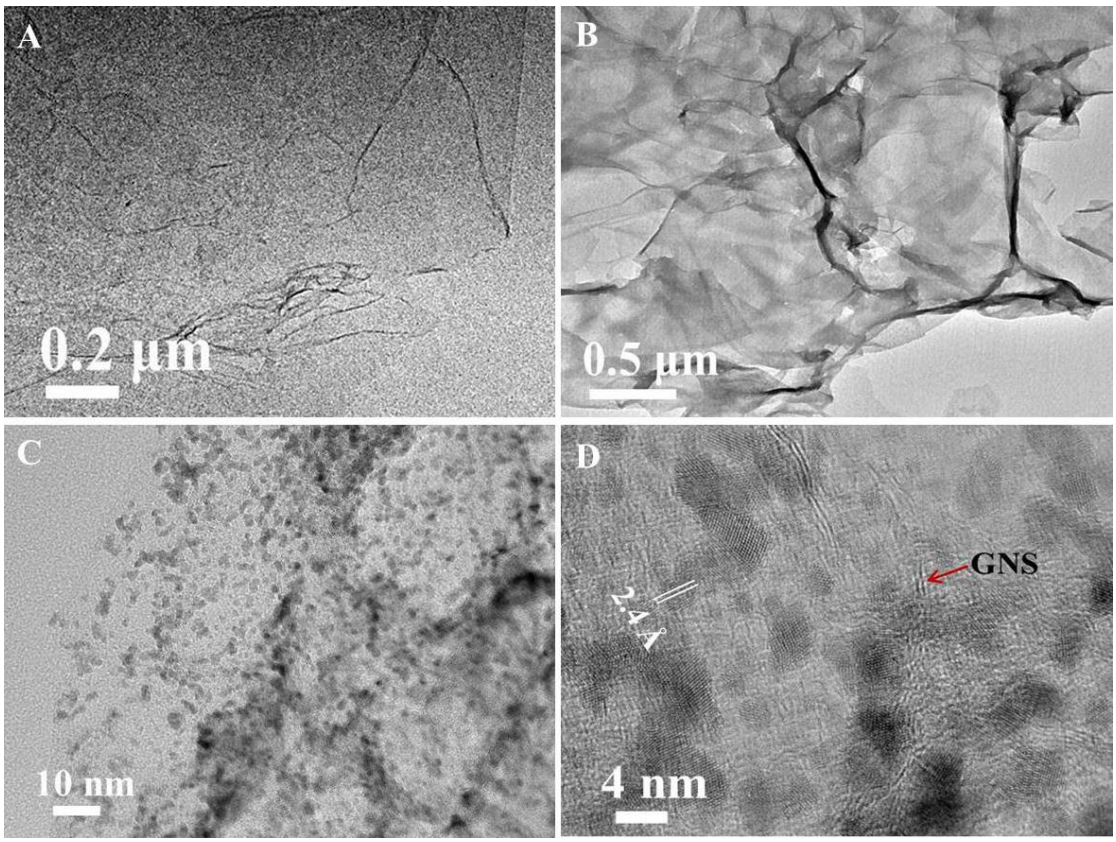

Figure 1. TEM images of (A) GNS, (B) PANI/GNS nanocomposites, (C) Pd/PANI/GNS nanohybrids, (D) HRTEM image of Pd/PANI/GNS nanohybrids

Then, the Pd NPs supported on PANI/GNS composites were used as template molecules to grow Pt NPs by the reduction of H_2PtCl_6. It is interestingly found that the structure of Pt-Pd bimetallic could be easily tuned *by* simply changing the reaction material. For example, Pt-Pd bimetallic with very few Pt nanobranches are adsorbed around Pd NPs onto the surface of PANI/GNS (sample 1), as shown in Figure 2A. When increasing the amounts of $H_2PtCl_6 \cdot 6H_2O$ to 0.52 mL (sample 2) under identical reaction conditions used for preparing sample 1. From Figure 2B we can see that the Pt-Pd bimetallic unevenly disperse onto the surface of PANI/GNS composites. When further increasing the amounts of $H_2PtCl_6 \cdot 6H_2O$ to 0.78 mL (sample 3) under identical reaction conditions used for preparing sample 1. Figure 2C reveal the globose flowered nanoparticles are successfully attached on the surface of PANI/GNS composites. And only a small number of Pt-Pd bimetallic form small branched structures. Figure 2D shows the image of Pt-Pd/PANI/GNS nanocatalysts which the amount of $H_2PtCl_6 \cdot 6H_2O$ is 1.0 mL 0.193 M (sample 4). It is reveals that the Pt-Pd bimetallic tends to aggregate together. The results further prove that Pt-Pd nanoflowers can be obtained *via* well-controlled reaction conditions.

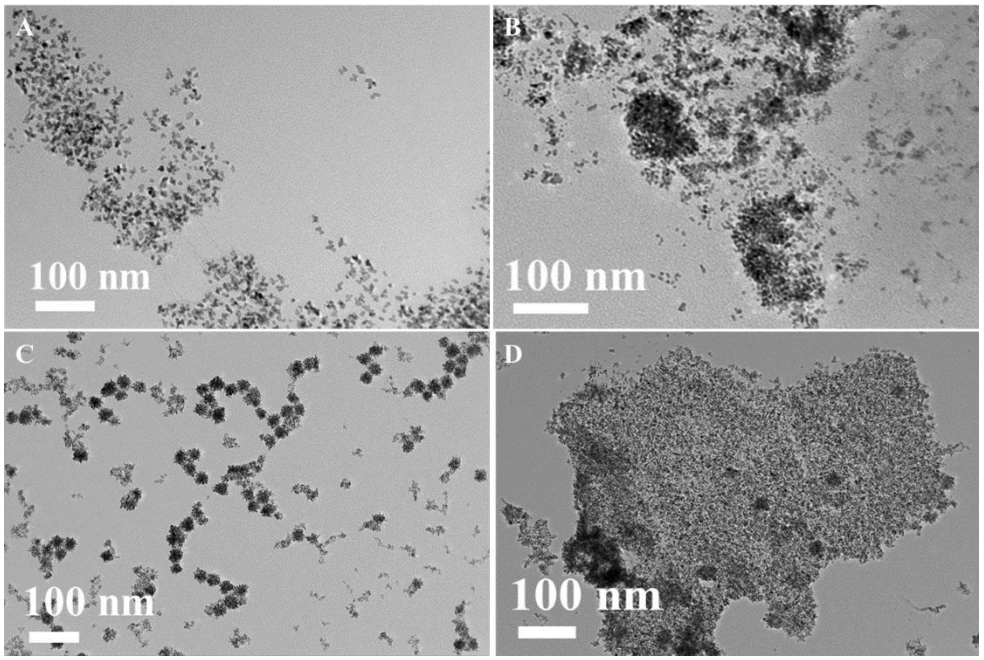

Figure 2. TEM images of Pt-Pd/PANI/GNS nanocatalysts at different reaction parameters. Reaction conditions: (A) 0.25 mL 1.0 M PVP, 0.26 mL 0.193 M $H_2PtCl_6 \cdot 6H_2O$, and 0.5 mL HCOOH, sample 1; (B) 0.5 mL1.0 M PVP, 0.52 mL 0.193 M $H_2PtCl_6 \cdot 6H_2O$, and 0.75 mL HCOOH, sample 2; (C) 0.75 mL 1.0 M PVP, 0.78 mL 0.193 M $H_2PtCl_6 \cdot 6H_2O$, and 1.0 mL HCOOH, sample 3; (D) 1.0 mL1.0 M PVP, 1.0 mL 0.193 M $H_2PtCl_6 \cdot 6H_2O$, and 1.25 mL HCOOH, sample 4.

Figure 3A shows the TEM images of 3D dendritic Pt-Pd/PANI/GNS nanocatalyst (sample 3). The results reveal that several Pt nanoparticles have grown center on the Pd core and form prominent branched structure. And many branched structures combine to form spikes of flowers. The Pt-Pd bimetallic nanoflowers have an average size of 25 nm. In order to further prove the clear structure of Pt-Pd bimetallic nanoflowers, HRTEM images of Pt-Pd/PANI/GNS nanocatalysts are shown in Figure 3B, which clearly reveal that the overgrowth of Pt nanobranches at multiple sites on the Pd seed. Each flower structure is composed of many Pt and Pd NPs. The Pt and Pd NPs have significant difference that the darker Pd center was grown several lighter Pt NPs in Pt-Pd bimetallic nanoflower. The Pt-Pd bimetallic nanoflowers actually have porous nanostructure. In order to further confirm the composition of prepared Pt-Pd/PANI/GNS nanocatalyst. The EDX spectrum was used to characterize the nanocatalyst. The result as shown in Figure 3C, which reveal the presence of C, N, O, Pt and Pd elements. These results also prove the successful synthesis of Pt-Pd/PANI/GNS nanocatalyst

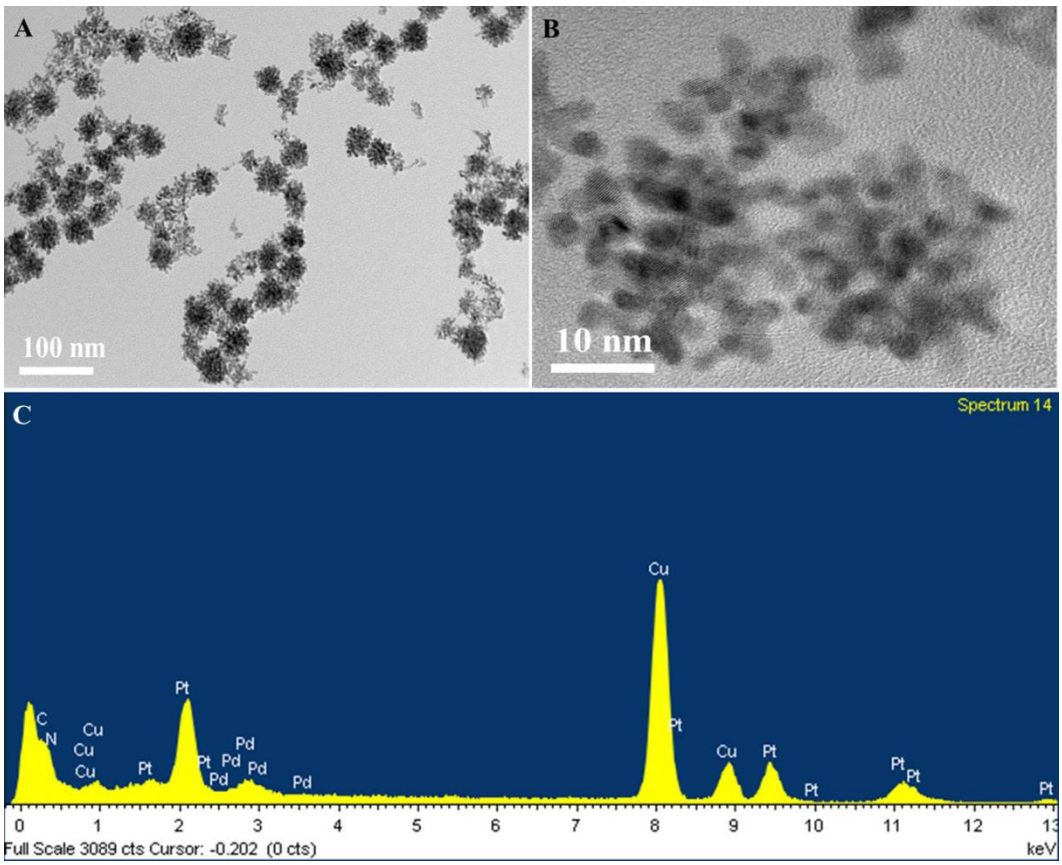

Figure 3. TEM (A) and HRTEM (B) images of Pt-Pd/PANI/GNS nanocatalyst (sample 3) at different magnifications. (C) EDX spectrum of Pt-Pd/PANI/GNS nanocatalyst (sample 3). Reaction conditions: 0.75 mL of PVP (1 M), 1.25 mL of HCOOH and 0.78 mL of H_2PtCl_6 (0.193 M).

Figure 4 shows the XRD graph of the obtained PANI/GNS nanocomposites and Pt-Pd/PANI/GNS nanocatalyst. The PANI/GNS nanocomposites show a broad diffraction peaks at $2\theta=25.2°$, corresponding to the graphite-like structure (002), and the peak is wider than the pure GNS which reported in the literature [20]. That further proves the PANI films have been successfully modified onto the surface of GNS. Figure 4b shows the XRD pattern of the Pt-Pd/PANI/GNS nanocatalyst. The characteristic diffraction peaks at 39.9°, 46.4°, 67.9°, and 81.6° which correspond to the (111), (200), (220), and (311) crystal planes of Pt-Pd bimetallic [21]. The average particle size can be calculated as about 25.3 nm by the Debye-Scherrer equation [18], which is in agreement with the results that obtained from HRTEM (Figure 3B).

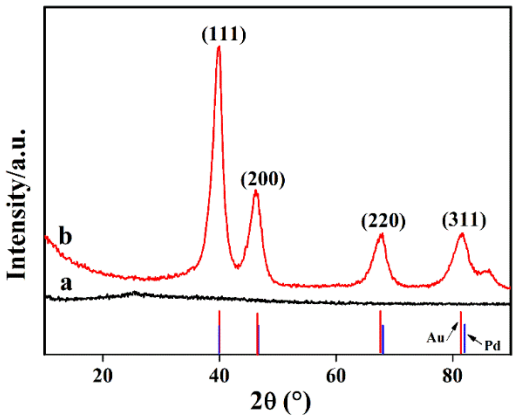

Figure 4. XRD patterns of a) GNS/PANI and b) Pt-Pd/PANI/GNS nanocatalyst (sample 3). Reaction conditions: 0.75 mL of PVP (1 M), 1.25 mL of HCOOH and 0.78 mL of H_2PtCl_6 (0.193 M).

3.2 Electrochemically active surface area

The electrochemical activity of nanocatalyst was evaluated by cyclic voltammogram (CV) experiments. The CV tests were carried out in N_2-saturated aqueous H_2SO_4 within the potential range from -0.2-1.2 V at a scan rate of 50 mV/s. Hydrogen adsorption/desorption peaks are usually used to calculate the ECSA of electrocatalysts [22]. The CV curves of Pt-Pd/PANI/GNS nanocatalyst which prepared with different reaction parameters are shown in Figure 5. The ECSA of Pt-Pd/PANI/GNS nanocatalyst were calculated. It is revealed that the ECSA values are 77.74 m^2/g for sample 3, 69.37 m^2/g for sample 4, 61.49 m^2/g for sample 2, and 57.19 m^2/g for sample 1, respectively. The results further reveal that the ECSA of Pt-Pd/PANI/GNS nanoflower is higher than the other Pt-Pd/PANI/GNS nanocatalyst. Moreover, the ECSA of Pt-Pd/PANI/GNS nanoflower is larger than the literature reported. For example, Pt/CCG for 36.27 m^2/g [22], GO-Pt for 16.9 m^2/g [23], Pt/SWCNT for 18.4 m^2/g [24], and Pd/G for 24.3 m^2/g [25]. That maybe due to the excellent structures and good dispersions of Pt-Pd nanoflowers. These results also prove that the obtained Pt-Pd/PANI/GNS nanoflowers possess excellent electrochemically activity.

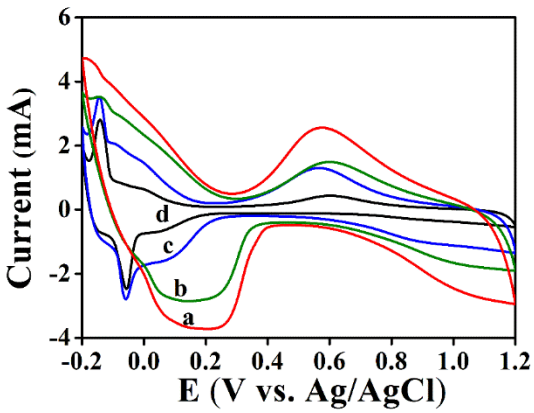

Figure 5. Electrochemical catalytic performances of Pt-Pd/PANI/GNS nanocatalysts in N_2-saturated aqueous H_2SO_4 (0.5 M) at a scan rate of 50 mV/s. (a) sample 3, (b) sample 4, (c) sample 2, (d) sample 1.

3.3 Methanol electro-oxidation

CVs for electro-oxidation of methanol performed in 0.5 M H_2SO_4 solution containing 1 M CH_3OH are shown in Figure 6A. The onset potential of methanol oxidation were about 0.32 V. The all CV curves show that the current peak about 0.77 V in the forward scan are attributed to methanol oxidation on Pt-Pd/PANI/GNS nanocatalysts. And the current peak about 0.59 V in the backward scan are attributed to the removal of the residual carbonaceous species [26]. The peak current of Pt-Pd/PANI/GNS nanoflower (sample 3) is higher than the other. This result indicates that the electrocatalytic activity of Pt-Pd/PANI/GNS nanoflower is obviously higher than the other, which is accord with the results of the ECSA. That maybe due to the particular morphology of Pt-Pd bimetallic nanoflower. The ratio of the forward anodic peak current (I_f) to the backward anodic peak current (I_b), I_f/I_b, can be used to describe the catalyst tolerance of the poisoning species accumulation [22]. The ratios for Pt-Pd/PANI/GNS are calculated to be 1.77, 2.09, 2.89, 2.54 for sample 1, sample 2, sample 3 and sample 4, respectively. The results further prove that Pt-Pd/PANI/GNS nanoflower (sample 3) has less carbonaceous accumulation. This indicates that Pt-Pd/PANI/GNS nanoflower (sample 3) possesses a higher catalytic activity for methanol oxidation.

The electrochemical long term stabilities of the nanocatalysts were also further investigated by chronoamperometric tests. Figure 6B shows the chronoamperometric curves of Pt-Pd/PANI/GNS nanocatalysts in 0.5 M H_2SO_4+1.0 M CH_3OH solution. It is observed that the Pt-Pd/PANI/GNS nanoflower (sample 3) exhibits a higher current than the other sample. It is noted that the current rapidly decline for all catalysts at the beginning of the chronoamperometric tests. These phenomenon will attributed to the generation toxic intermediates during the incomplete oxidation of methanol and then the intermediates adsorbed on the nanocatalysts surface, covering the active site surfaces [25]. The Pt-Pd/PANI/GNS nanoflower (sample 3) shows more resistance to current decay compared to the other catalysts after this fast decay.

Table 1. Comparison of the catalytic activity of each catalyst toward methanol oxidation.

catalysts	surface area (m^2/g)	I_f/I_b	reference
Pt/CCG	36.27	0.83	[22]
GO-Pt	16.9	--	[23]
Pt/SWCNT	18.4	--	[24]
Pd/G	24.3	1.3	[25]
Pt-Pd/PANI/GNS (sample 2)	61.49	2.89	This work

The current density for Pt-Pd/PANI/GNS nanocatalysts are 0.74 mA/mg for sample 4, 0.83 mA/mg for sample 3, 0.68 mA/mg for sample 2, and 0.44 mA/mg for sample 1, respectively. These results prove that the electrocatalytic activity and stability of Pt-Pd/PANI/GNS nanoflower (sample 3) is much better than the other nanocatalysts. The high electrochemical activity and stability of Pt-Pd/PANI/GNS nanoflower (sample 3) is most likely due to the excellent floral structure. There are a lot of pore structures in Pt-Pd/PANI/GNS nanoflower that maybe benefit for electrode transfer. Also we obtained Pt-Pd/PANI/GNS nanocatalyst is show excellent electrocatalytic activity for methanol oxidation compared with the literature reported. The results are show in Table 1.

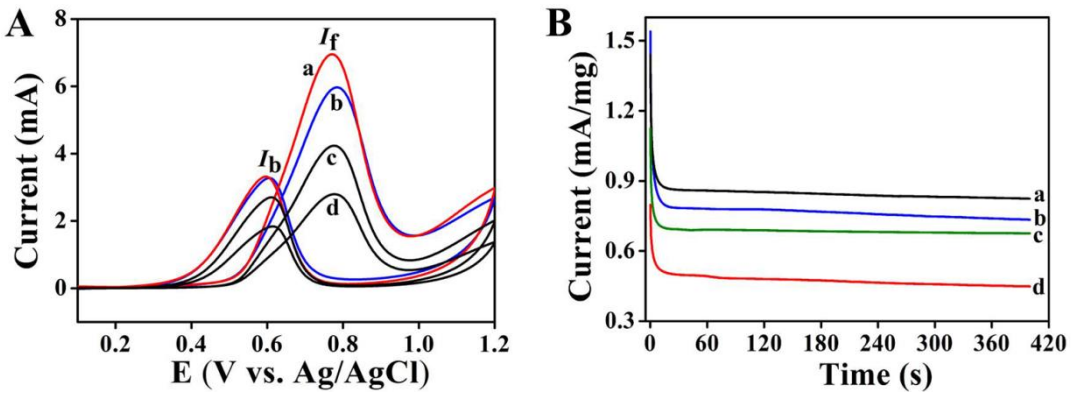

Figure 6. Cyclic voltammogram (A) and Chronoamperometric curves (B) of Pt-Pd/PANI/GNS nanocatalysts-modified GCE in aqueous CH_3OH (1 M)+H_2SO_4 (0.5 M) at 20 mV/s. (a) sample 3, (b) sample 4, (c) sample 2, (d) sample 1

The electrocatalytic activity of Pt-Pd/PANI/GNS nanocatalysts has been researched for oxygen reduction reaction. Figure 7 shows the typical CVs of oxygen reduction at the Pt-Pd/PANI/GNS-modified GCE in a 1.0 M H_2SO_4 solution in saturated oxygen. A remarkable catalytic reduction current can be observed at 0.49 V in all Pt-Pd/PANI/GNS nanocatalysts. The reduction peak current increases gradually when increase the amount of Pt precursors. It's worth noting that the nanocatalysts with high-density Pt nanodendrites modified GCE exhibits higher electrocatalytic current for dioxygen reduction (Figure 7a, sample 3) than the other sample with the low-density one. Unfortunately, the reduction peak current declines instead of increases when the amount of Pt precursor is highest than the other samples. That maybe due to the Pt-Pd/PANI/GNS nanocatalysts which tend to aggregation have a poor electrochemical activity. Furthermore, the reduction peak potential occursed at 0.49 V of Pt-Pd/PANI/GNS nanoflower (sample 3) modified GCE is significantly more positive than the reported catalysts. For instance, Crooks reported that the dendrimer-encapsulated Pt-modified electrode shows the reduction peak at 0.25 V [27]. Wang reported that the Au/Pt hybrid NPs-modified electrode shows the reduction peak at 0.4 V [28]. The results further show that Pt-Pd/PANI/GNS nanoflower has excellent electrocatalytic activity for methanol oxidation. And the comparison results are show in Table 1.

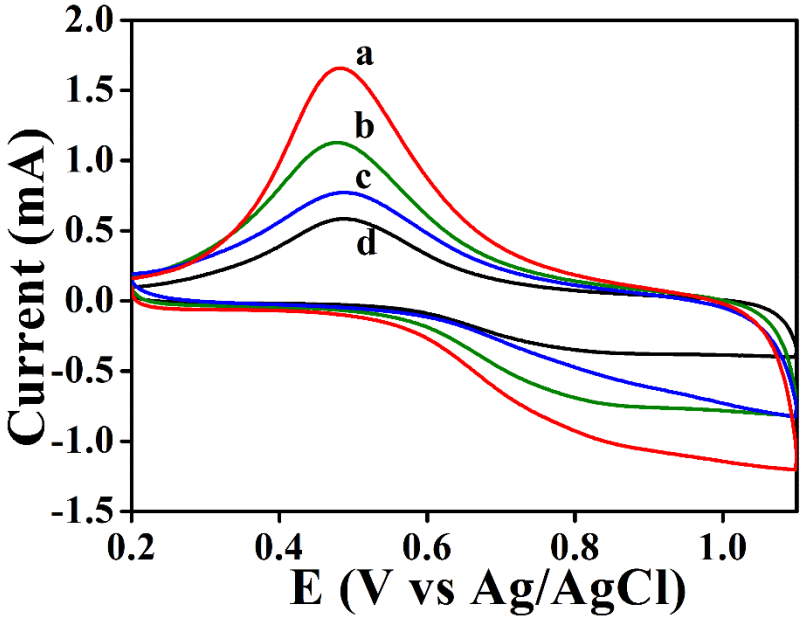

Figure 7. Cyclic voltammogram of oxygen reduction at Pt-Pd/PANI/GNS nanocatalysts-modified GCE in H_2SO_4 (1.0 M) + saturated O_2 at 20 mV/s.

4. CONCLUSION

In summary, we have designed a facile procedure to prepare Pt-Pd/PANI/GNS nanocatalyst. The Pt-on-Pd bimetallic with controllable shape can be obtained *via* changing the reaction parameter. Most importantly, the nanoflowered Pt-Pd bimetallic supported on PANI/GNS have a much higher ECSA and catalytic activity than the other structured Pt-Pd/PANI/GNS nanocatalysts. We prepared nanoflowered Pt-Pd/PANI/GNS nanocatalysts show excellent electrochemical catalyst activity toward methanol oxidation and oxygen reduction.

ACKNOWLEDGEMENTS
This work was supported by the National Natural Science Foundation of China (No. 21665008), Youth project of Yunnan Province (No 2014FD054), the Scientific Research Fund Project of Honghe University (XJ14Z02).

References

1. Y. J. Hu, H. Z. Hang, P. Wu, H. Zhang, B. Zhou, and C. Cai, *Phys. Chem. Chem. Phys.*, 13 (2011) 4083.
2. Y. Zuo, Y. P. Liu, J. S. Li , R. F. Du, X. T. Yu, C. C. Xing, T. Zhang, L. Yao, J. Arbiol, J. Llorca, K. Sivula, N. Guijarro and A. Cabot, *ACS Appl. Mater. Interfaces*, 11 (2019) 6918.
3. H. Xu, A. L. Wang, Y. X. Tong and G. R. Li, *ACS Catal.*, 6 (2016) 5198.
4. S. J. Guo, S. J. Dong and E. K. Wang, *ACS Nano*, 4 (2010) 547.
5. S. Su, C. Zhang, L. H. Yuwen, X. F. Liu, L. H. Wang, C. H. Fan and L. H. Wang, *Nanoscale*, 8 (2016) 602.

6. Y. J. Guo, S. J. Guo, J. T. Ren, Y. M. Zhai, S. J. Dong and E. K. Wang, *ACS Nano*, 4 (2010) 4001.
7. Y. Si and E. T. Samulski, *Nano Lett.*, 8 (2008) 1679.
8. S. J. Park, J. An, I. Jung, R. D. Piner, S. J. An, X. S. Li, A. Velamakanni and R. S. Ruoff, *Nano Lett.*, 9 (2009) 1593.
9. S. Stankovich, R. D. Piner, X. Q. Chen, N. Q. Wu, S. T. Nguyen and R. S. Ruoff, *J. Mater. Chem.*, 16 (2006) 155.
10. Y. N. Li, J. Cheng, L. Q. Hu, J. Z. Liu , J. H. Zhou and K. F. Cen, *Energy Fuels*, 32 (2018) 6918.
11. M. Shekhirev, P. Zahl and A. Sinitskii, *ACS Nano* 12 (2018) 8662.
12. S. J. Park, D. A. Dikin, S. T. Nguyen and R. S. Ruoff, *J. Phys. Chem. C*, 113 (2009) 15801.
13. H. Yu, H. Han, J. Jang and S. Cho, *ACS Omega*, 4 (2019) 5586.
14. R. S. Diggikar, S. P. Deshmukh, T. S. Thopate and S. R. Kshirsagar, *ACS Omega*, 4 (2019) 5741.
15. C. C. Li, D. B. Liu, Y. K. Xiao, Z. X. Liu, Li Song and Z. P. Zhang, *ACS Appl. Energy Mater.*, , (2019).
16. W. S. Hummers and R. E. Offeman, *J. Am. Chem. Soc.*, 80 (1958) 1339.
17. L. J. Cote, F. Kim and J. X. Huang, *J. Am. Chem. Soc*, 131 (2009) 1043.
18. J. D. Qiu, L. Shi, R. P. Liang, G. C. Wang and X. H. Xia, *Chem. Eur. J*, 18 (2012) 7950.
19. D. C. Wei, Y. Q. Liu, Y. Wang, H. L. Zhang, L. P. Huang and G. Yu, *Nano Lett.*, 9 (2009) 1752.
20. J. Yan, T. Wei , B. Shao, Z. J. Fan, W. Z. Qian, M. L. Zhang and F. Wei, *Carbon*, 48 (2010) 487.
21. C. Singhala, C. S. Pundirb and J. Narang, *Biosens. Bioelectron.*, 97 (2017) 75.
22. Y. J. Li, W. Gao, L. J. Ci, C. M. Wang and P. M. Ajayan, *Carbon*, 48 (2010) 1124.
23. B. Seger and P. V. Kamat, *J. Phys. Chem. C* 113 (2009) 7990
24. A. Kongkanand, S. Kuwabata, G. Girishkumar and P. Kamat, *Langmuir*, 22 (2006) 2392.
25. M. Dehvari, H. Saravani, N. Akbarzadeh and M. Z. Yazdan-Abad, *International Journal of Hydrogen Energy*, 44 (2019) 6544.
26. M. C. Lima dos Santos, R. M. Dutra, V. A. Ribeiro, E. V. Spinacé and A. O. Neto, *Int. J. Electrochem. Sci.*, 12 (2017) 3549.
27. H. C. Ye and R. M. Crooks, *J. Am. Chem. Soc.*, 127 (2005) 4930.
28. S. J. Guo, L. Wang, S. J. Dong and E. K. Wang, *J. Phys. Chem. C* 112 (2008) 13510.